厚生労働科学研究費補助金（萌芽的先端医療技術推進研究事業）
分担研究報告書

超音波を利用したsiRNA内包バブルリポソームのがん局所療法の臨床試験導入

分担研究者　福岡大学　医学部解剖学教室　立花克郎

研究要旨
標的バブルリポゾームに最適化された低侵襲治療装置の開発

A.　研究目的

超音波エネルギーによる，生体作用、薬剤透過性亢進作用、細胞内遺伝子導入、など、既に多くの論文で最近報告されてきた。本研究の目的は、超小型の超音波発振セラミック技術を応用した超音波照射による遺伝子導入の検討およびその安全な低侵襲治療システムの確立にある。

B. 研究方法

超音波発振プローブを用い特注の膜式細胞培養容器の近くで超音波照射し、癌細胞に対する影響は最小限に押さえ、かつ、培養細胞の位置している目標の部位で容易に遺伝子導入ができる実験方法を開発した。in vitroでの、HeLa癌細胞株で超音波単独照射を行いの殺細胞効果およびアポトーシスを検討した。超音波条件はPZTの素子（20ミリ径　ディスク型）超音波プローブに絶縁性が高い材質で被覆し、電圧を負荷し（最大100ボルト)、超音波エネルギーを測定した。脱気水に満たされたタンクの中に超音波プローブとともに一定の距離にて0.8MHzから1.6MHzの周波数を順次負荷させ、超音波強度の分布も観測した。この条件を各超音波条件（周波数、強度、照射距離）に対応させてマイクロバブルと併用して遺伝子導入率を測定した。マイクロバブルの種類は市販のエコーコントラスト剤レボビスト(Levovist)、オプチゾン(Optison)を使用した。

（倫理面への配慮）
特に問題なし

C. 研究結果

特注の超音波発振プローブを用いた膜式細胞培養容器では通常の回転式試験管超音波照射方式に比べ著しく細胞殺傷率の低下が認められた。また、膜式細胞培養容器の超音波照射後方に超音波吸収材の有無で2—3倍の違いがあった。一方、超音波周波数、強度、パルス、Duty factorをそれぞれの条件を変位させても同様の傾向が認められ、超音波照射の環境に依存した。アポトーシスはAnnexin V-FITC染色法を用い測定したところPRF

0.5Hz、Duty factor２５％、周波数変位幅を1.011MHz を中心に 12%振った条件で最もアポトーシス誘発が著明であった。超音波強度の増加によってネクローシスが著明になるにつれ、アポトーシスは認められなくなり、0.5-1.2W/cm2 でアポトーシスのピークが認められた。Annexin V-FITC 染色法および PI 染色ほの併用で測定したところ、前者で16.5%、後者で5.9%の細胞染色率が認められ、超音波の条件にかかわらず両者が染色された細胞が多く存在した。マイクロバブルの種類の違いは今回の実験条件では優位な差は認められなかった。一方、前記の超音波条件下での遺伝子導入率実験ではアポトーシス、ネクローシスの誘発率との解離的な現象は観測されなず、5-10%の遺伝子導入率にとどまった。使用された 20 ミリ直径の超音波プローブで周波数を変えたところ、1.011mHz を中心に 12%前後に変化させたところ、中心周波数のピーク消費電力の 50%近い減少が認められた。しかし、本実験では４個の20ミリ素子を並列に使用したので、細胞殺傷率では超音波変化させた群が優位に安定した、再現性の高い結果が得られた。

D. 考察

本実験で特別に開発された膜式細胞培養器は安定的に細胞に及ぼす超音波の影響が正確に観測できた。容器の超音波照射面の後方に設置された音響吸収材で完全に standing wave を防げたと思われる。Annexin V-FITC 染色法および PI 染色の両方に染色された細胞は二次的なアポトーシスを誘発したと考えられ、初期にアポトーシスを経て最終的に細胞死したと予想される。今回、バブルの厳密な種類と濃度の実験はなられんかったので今後、この測定システムを利用した詳しい条件設定の検討が必要である。

E. 結論

本実験結果より超音波の細胞への影響、遺伝子導入率、バブルの超音波条件設定を検討する上で必要な実験システムが開発されたと考えられる。様々な超音波条件よるアポトーシス、遺伝子導入率の比較検討が行われたが、今後さらにこの実験方法で超音波プローブ最適条件の再検討と新しいマイクロバブルの研究開発が期待される。

F. 健康危険情報

特になし

G. 研究発表

1. 論文発表

1. Sonoda S, Tachibana K, Uchino E, Okubo A, Yamamoto M, Sakoda K, Hisatomi T, Sonoda KH, Negishi Y, Izumi Y, Takao S, Sakamoto T. Gene transfer to corneal epithelium and keratocytes mediated by ultrasound with microbubbles. Invest Ophthalmol Vis Sci. 47(2):558-64, 2006

2. Sivakumar M, Tachibana K, Pandit AB, Yasui K, Tuziuti T, Towata A, Iida Y. Transdermal drug delivery using ultrasound-theory, understanding and critical analysis. Cell Mol Biol

(Noisy-le-grand). 2;51Suppl:0L767-84, 2006
3. Koike H, Tomita N, Azuma H, Taniyama Y, Yamasaki K, Kunugiza Y, Tachibana K, Ogihara T, Morishita R. An efficient gene transfer method mediated by ultrasound and microbubbles into the kidney. J Gene Med. 7(1):108-16, 2005

2. 学会発表

H. 知的財産権の出願・登録状況

1. 特許取得
   特になし
2. 実用新案登録
   特になし
3. その他
   特になし

別紙４

研究成果の刊行に関する一覧表レイアウト（参考）

書籍

著者氏名	論文タイトル名	書籍全体の編集者名	書　籍　名	出版社名	出版地	出版年	ページ

雑誌

発表者氏名	論文タイトル名	発表誌名	巻号	ページ	出版年
Y Bae, Matsumura Y, et al.	Preparation and biological characterization of polymeric micelle drug carriers with intracellular pH-Triggered Drug Release property: tumor permeability, controlled subcellular drug distribution, and enhanced in vivo antitumor efficacy.	Bioconjugate Chem.	16	122-130	2005
T Hamaguchi, Y Matsumura, et al.	NK105, a paclitaxel-incorporating micellar nanoparticle formulation, can extend in vivo antitumour activity and reduce the neurotoxicity of paclitaxel.	Brit J Cancer.	92	1240-1246	2005
H Uchino, Y Matsumura et al.	Cisplatin-Incorporating Polymeric Micelles (NC-6004) Can Reduce Nephrotoxicity and Neurotoxicity of Cisplatin in Rats.	Brit J Cancer.	93	678-687	2005
K. Sawada, Y.Furuichi, et al.	Differential cytotoxicity of anticancer agents in pre- and post-immortal lymphoblastoid cell lines.	Biol.Pharm.Bull.	28	1202-1207	2005
K. Futami, Y. Furuichi et al.	Quantitative analysis of Werner helicase activity using the single-molecule fluorescence detection system MF10S.	Biol.Pharm.Bull.	28	9-12	2006

Sonoda S, Tachibana et al.	Gene transfer to corneal epithelium and keratocytes mediated by ultrasound with microbubbles.	Invest Ophthalmol Vis Sci.	47	558-564	2006
Sivakumar M, Tachibana K et al.	Transdermal drug delivery using ultrasound-theory, understanding and critical analysis.	Cell Mol Biol (Noisy-le-grand).	2;51 Suppl	0L767-84	2006
Koike H, Tachibana K et al.	An efficient gene transfer method mediated by ultrasound and microbubbles into the kidney.	J Gene Med.	7	108-116	2005
Koshiyama K, Kodama T, et al.	Molecular delivery into a lipid bilayer with a single shock wave using molecular dynamics simulation.	AIP (American Institute of Physics) Conference Proceedings.	754	104-106	2005

Preparation and Biological Characterization of Polymeric Micelle Drug Carriers with Intracellular pH-Triggered Drug Release Property: Tumor Permeability, Controlled Subcellular Drug Distribution, and Enhanced in Vivo Antitumor Efficacy

Younsoo Bae, Nobuhiro Nishiyama, Shigeto Fukushima, Hiroyuki Koyama, Matsumura Yasuhiro, and Kazunori Kataoka

Department of Materials Science and Engineering, Graduate School of Engineering, The University of Tokyo, 7-3-1 Hongo, Bunkyo-ku, Tokyo 113-8656, Japan, Department of Clinical Vascular Regeneration, Graduate School of Medicine, The University of Tokyo, 7-3-1 Hongo, Bunkyo-ku, Tokyo 113-8655, Japan, and Investigative Treatment Division, National Cancer Center Research Institute East, 6-5-1 Kashiwanoha, Kashiwa, Chiba 277-8577, Japan

Bioconjugate Chemistry®

Reprinted from
Volume 16, Number 1, Pages 122–130

Preparation and Biological Characterization of Polymeric Micelle Drug Carriers with Intracellular pH-Triggered Drug Release Property: Tumor Permeability, Controlled Subcellular Drug Distribution, and Enhanced in Vivo Antitumor Efficacy

Younsoo Bae,[†] Nobuhiro Nishiyama,[‡] Shigeto Fukushima,[†] Hiroyuki Koyama,[‡] Matsumura Yasuhiro,[§] and Kazunori Kataoka*,[†]

Department of Materials Science and Engineering, Graduate School of Engineering, The University of Tokyo, 7-3-1 Hongo, Bunkyo-ku, Tokyo 113-8656, Japan, Department of Clinical Vascular Regeneration, Graduate School of Medicine, The University of Tokyo, 7-3-1 Hongo, Bunkyo-ku, Tokyo 113-8655, Japan, and Investigative Treatment Division, National Cancer Center Research Institute East, 6-5-1 Kashiwanoha, Kashiwa, Chiba 277-8577, Japan. Received July 28, 2004; Revised Manuscript Received October 31, 2004

A novel intracellular pH-sensitive polymeric micelle drug carrier that controls the systemic, local, and subcellular distributions of pharmacologically active drugs has been developed in this study. The micelles were prepared from self-assembling amphiphilic block copolymers, poly(ethylene glycol)-poly(aspartate hydrazone adriamycin), in which the anticancer drug, adriamycin, was conjugated to the hydrophobic segments through acid-sensitive hydrazone linkers. By this polymer design, the micelles can stably preserve drugs under physiological conditions (pH 7.4) and selectively release them by sensing the intracellular pH decrease in endosomes and lysosomes (pH 5–6). In vitro and in vivo studies show that the micelles have the characteristic properties, such as an intracellular pH-triggered drug release capability, tumor-infiltrating permeability, and effective antitumor activity with extremely low toxicity. The acquired experimental data clearly elucidate that the optimization of both the functional and structural features of polymeric micelles provides a promising formulation not only for the development of intracellular environment-sensitive supramolecular devices for cancer therapeutic applications but also for the future treatment of intractable cancers with limited vasculature.

INTRODUCTION

The selective augmentation of drug concentrations in avascular tumor tissues is the most challenging issue of current cancer chemotherapy using macromolecular bioconjugates (*1*–*3*). Most anticancer drugs are pharmacologically effective but limited in their clinical applications due to serious toxicity and low water solubility; thereby, the altered biodistribution of these drugs has an important meaning not only to reduce the toxicity but also to improve therapeutic effects (*4*–*6*). For these reasons, interest has centered on the creation of drug carriers that safely and precisely deliver the appropriate amounts of active drugs to solid tumors (*7*–*10*). Indeed, several macromolecular drug carriers are under clinical trials or used practically, which include water-soluble polymer–drug conjugates (*11*), liposomal carriers (*12*), and polymeric micelles (*13*). However, even though these carriers have made significant advancements in cancer therapy, recent studies point out their antitumor activities are subject to change according to the cancer species with pathological, pharmacological, and biochemical differences (*14*).

There are three major reasons why the present macromolecular drug carriers have difficulties in clinical use. First, the carriers injected into the body encounter in vivo barriers such as nonspecific systemic accumulation and phagocytotic clearance by the host defense system (*15*). Second, even after the carriers accumulated in solid tumors avoiding these in vivo barriers, they still have to overcome the heterogeneous tumor microenvironments that are characterized by insufficient blood supply, disordered vasculatures, and diffusion-limited interstitum (*16*). Third, the carriers that successfully accessed the inside of tumor tissues should release the loaded drugs back into active forms in order to exert the antitumor effect (*17*). Among these reasons, poor permeability of the carriers inside the tumor tissues and low concentrations of active drugs throughout solid tumors become particularly serious problems (*18, 19*). For these reasons, understanding the correlation between the physicochemical properties of drug carriers and their behaviors in the body is very important, and the combination of these two features is required for the design of ultimate carriers (*20*).

In this article, we will report that such tantalizing problems may be overcome by a novel tumor-infiltrating drug carrier, the pH-sensitive polymeric micelle, whose structural and functional features were optimized for the intracellular drug delivery (Figure 1A). The micelle is a nanosized supramolecular assembly from the self-assembling amphiphilic block copolymers, poly(ethylene glycol)-poly(aspartate hydrazone adriamycin) [PEG-p(Asp-Hyd-ADR)]. The anticancer drug, adriamycin (ADR), is

* To whom correspondence should be addressed. Phone: +81-3-5841-7138, Fax: +81-3-5841-7139, E-mail: kataoka@bmw.t.u-tokyo.ac.jp.

[†] Department of Materials Science and Engineering, The University of Tokyo.

[‡] Department of Clinical Vascular Regeneration, The University of Tokyo.

[§] National Cancer Center Research Institute East.

10.1021/bc0498166 CCC: $30.25
Published on Web 12/22/2004

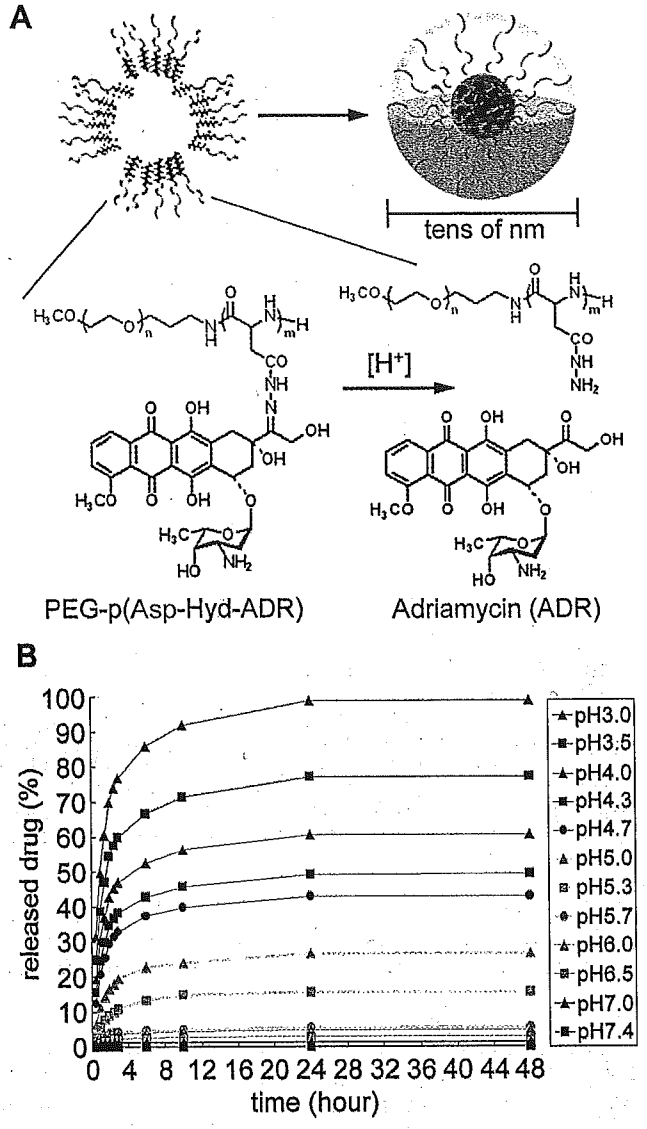

Figure 1. Preparation of tumor-infiltrating polymeric micelles with intracellular pH-sensitivity. (A) Micelles with tens of nm size diameter were prepared from self-assembling amphiphilic block copolymers, PEG-p(Asp-Hyd-ADR), in which the anticancer drug, adriamycin (ADR), was conjugated through acid-sensitive hydrazone linkers. (B) The micelles released the loaded drugs under acidic conditions below pH 6.0 corresponding to intracellular space, but remained stable under the conditions of vascular and extracellular space (pH 7.4–7.0).

conjugated to the core-forming segments through the hydrazone linkers that are stable under physiological conditions (pH 7.4) but cleavable under acidic intracellular environments in endosomes and lysosomes (pH 5–6). This carrier design allows the micelle to safely protect hydrophobic drugs from the host defense system in the body and to selectively exert cytotoxicity due to intracellular pH-triggered drug release, improving both the delivery effect and therapeutic efficacy of the drugs (*21*). Therefore, the characteristic in vitro and in vivo behaviors of the micelles would offer intriguing information taking into account the future design and development of bioresponsive supramolecular carrier systems for the intracellular trafficking of biologically active molecules.

EXPERIMENTAL PROCEDURES

Materials. β-Benzyl-L-aspartate was from Sigma and α-methoxy-ω-amino poly(ethylene glycol) (PEG; MW = 12 000) was from Nippon Oil & Fats, Japan. PEG was purified using an ion-exchange gel column (CM-Sephadex C-50, Amersham Pharmacia Biotech) prior to the synthesis of the block copolymers. Adriamycin hydrochloride-(ADR–HCl) was from Nippon Kayaku, Japan, and its purity was checked by reversed phase liquid chromatograpy (RPLC). Sephadex LH-20 gel was from Amersham Pharmacia Biotech, Sweden.

Cell Lines and Animals. A human small cell lung cancer cell line SBC-3 and murine colon adenocarcinoma 26 (C26) cells were from the National Cancer Center Research Institute, Japan, and cultured in a medium (DMEM, Sigma, St. Louis, MO) containing 10% fetal bovine serum in a humidified atmosphere with 5% CO_2 at 37 °C. CDF-1 mice (female, 6 weeks old) were from Charles River, Japan. The animals were cared for and all experiments were performed in compliance with the Guide for the Care and Use of Laboratory Animals as adopted and promulgated by the National Institutes of Health.

Preparation of the pH-Sensitive Polymeric Micelles. The self-assembling amphiphilic block copolymer, PEG-p(Asp-Hyd-ADR), was synthesized as reported elsewhere (*22*). Briefly, poly(ethylene glycol)-poly(β-benzyl-L-aspartate) (PEG-PBLA) was synthesized from the ring-opening polymerization of β-benzyl-L-aspartate *N*-carboxyanhydride using PEG as a macro initiator, followed by substitution of the benzyl groups of PEG-PBLA with hydrazide groups for drug binding (see also Supporting Information). Unbound ADR was completely removed using Sephadex LH-20 gel, and the obtained polymers were redissolved in dimethylacetamide to prepare the micelle by a dialysis method.

Evaluation of Acid-Sensitive Drug Release from the Micelles. Reversed phase liquid chromatograpy (RPLC) analysis, using a μ-Bondasphere 5 μm C4-300A column (Nihon Waters, Japan), was used to assess the pH sensitivity of the micelle. The micelle with a 10 mg/mL concentration was incubated under various buffered conditions from pH 7.4 to 3.0 [20 mM phosphate buffer (pH 7.4–6.0), 20 mM acetate buffer (pH 5.8–3.0)], and time- and pH-dependently released drugs were measured from the peak intensity by a UV detector (485 nm).

Observations on Intracellular Drug Release and Localization of the Micelles. Multicellular tumor spheroid (MCTS) was prepared from a C26 cell line using a spheroid culture plate, Sumiloncelltight (Sumitomo Bakelite, Japan); 200 μm size MCTS were sorted and used for the experiments. Fluorescence images were observed using a confocal laser scanning microscope (LSM 510, Carl Zeiss, Germany) with a 20× objective (Plan-Apochromat, Carl Zeiss, Germany) and a 63× objective (C-Apochromat, Carl Zeiss, Germany) at excitation wavelengths of 488 nm (Ar laser) and 364 nm (UV laser) for ADR and Hoechst 33258, respectively. The concentrations of the micelles in the medium were adjusted to 10 μg/mL (ADR equivalent). All images were acquired and processed with the accompanying software.

In Vitro Growth Inhibition Assay. A tetrazolium dye method, called the MTT assay, was used to evaluate the growth-inhibitory effect of the micelle. Using 96-well culture plates, exponentially growing SBC-3 cells were seeded (2000 cell/well) and preincubated for 24 h, followed by coincubation with ADR and the micelle samples. After exposure for 3, 10, and 24 h, the medium was discarded and each cell was reincubated in fresh medium for another 24 h. The cells were then counted using a Bio-RAD Microplate Reader 550 (Bio-Rad Laboratories Inc.).

In Vivo Antitumor Activity and Body Weight Change of Mice. The antitumor activity of the micelles was evaluated with tumor bearing, 7-week-old, female SPF CDF1 mice (n = 6, Charles River, Japan). After implanting C26 cells 10 days earlier, injection of the samples took place using a volume of 0.1 mL/10 g body weight. The regimens of the micelles were scheduled by changing the administration dose (20, 40, and 60 mg/kg) three times with a 4-day interval, based on the optimized regimens of ADR as a control. However, in the case of ADR, only limited doses (5, 10, and 15 mg/kg) were applied to the mice due to the drugs toxicity. The mice were monitored daily, and tumor growth and body weights were measured at 2-day intervals. Tumor volume is calculated as follows: volume = $1/2 \times LW^2$ (L is the long diameter and W is the short diameter of a tumor).

Biodistribution and Pharmacokinetics. The CDF1 mice (n = 6), when the tumor volume reached ca. 100 mm^3, were injected with ADR and the micelles in a volume of 0.1 mL/10 g body weight for the experiments. The dose was either 10 mg/kg for ADR or the micelles (ADR equivalent). After the injection, blood, tumor, and major organs (heart, kidney, liver and spleen) were collected at 0.5, 1, 3, 6, 9, 24, and 48 h, followed by HPLC anaylsis (see Supporting Information for the detailed protocol).

Fluorescence Microscopic Observations of Solid Tumors and Their Peripheral Blood Vessels. The tumor-bearing mice were sacrificed at 24 h after the injection of the micelles with a 10 mg/kg dose. The intact tumor tissues with their peripheral blood vessels were harvested for macroscopic observations using a fluorescence microscope (Axiovert 200, Carl Zeiss, Germany) equipped with a 2.5× objective (Plan-Neofluar, Carl Zeiss, Germany) and a filter set15 (BP546/12, FT580, LP590, mercury lamp excitation, Carl Zeiss, Germany).

RESULTS

Preparation of the Intracellular pH-Sensitive Polymeric Micelles. The polymer backbone of PEG-p(Asp-Hyd-ADR) consisted of poly(ethylene glycol) (PEG) with a molecular weight of 12 000 g/mol for the hydrophilic shell-forming segment and 37 repeating units of polyaspartate (PAsp) for the core-forming segment (MW = 28 679), which were determined by gel permeation chromatography and ^{1}H NMR measurements. The 28 side chains in the PAsp block were replaced by hydrazide groups for the binding of the drugs. Adriamycin (ADR) was then conjugated to the polymer backbone through hydrazone bonds between the carbonyls at the C13 of ADR and the hydrazide groups of the PEG-p(Asp-Hyd) block copolymer. Even though the biological and chemical background of binding ADR to polymer backbone through hydrazone linkages has been delineated in our previous work (*22*) as well as many studies (*23*–*26*), it must be noticed that the hydrazone linkage is the most popularly used as pH-sensitive linkers due to the fact that this bond is quite stable at pH 7.4 but hydrolyzes under mild acidic conditions with pH 5–6. Therefore, to ensure that drug release from the micelles occurs only when acid-labile hydrazone linkers are cleaved, any unbound free ADR were completely removed in this study. These were confirmed by a reversed phase liquid chromatograpy (RPLC) analysis that is generally used for separating and purifying materials due to the differences in their hydrophobic properties (further details are described below). RPLC analysis showed the drug loading content of PEG-p(Asp-Hyd-ADR) was 42.5 wt % with respect to a single block copolymer chain. The obtained PEG-p(Asp-Hyd-ADR) block copolymers self-assembled into micelles in aqueous solutions; the prepared micelles had a 65 nm diameter, which was confirmed by dynamic light scattering measurements.

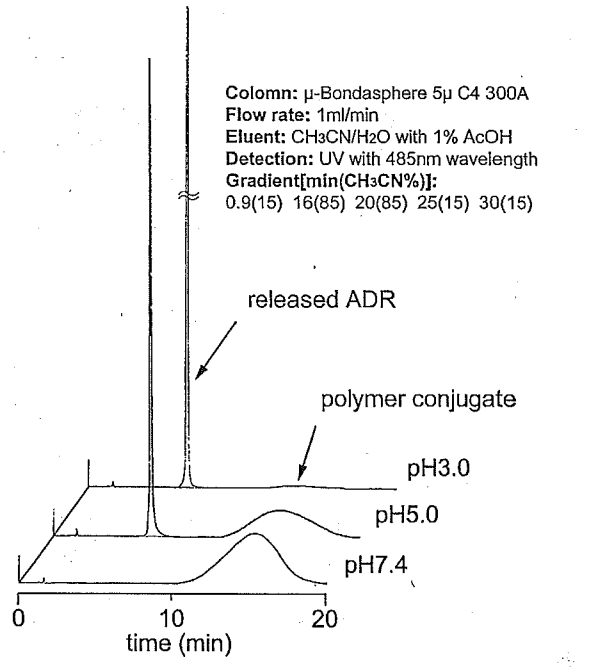

Figure 2. Acid-sensitive cleavage of drug-binding hydrazone bonds evaluated by reversed phase liquid chromatography (RPLC) analysis. RPLC separates free drugs and polymer conjugates due to the differences in their hydrophobic properties, demonstrating absence of free drugs at pH 7.4 possibly binding to polymer conjugates in a physical way. On the other hand, it clearly shows that the amount of released drugs increases under acidic conditions in which the drug-binding hydrazone linkers can be cleaved.

The Micelles Selectively Release the Loaded Drugs by Sensing a pH Decrease. To confirm the acid-sensitive drug release profile, the micelles were incubated under various pH conditions from 7.4 to 3.0, and the released drugs were measured using RPLC analysis. Figure 1B shows that the micelles released the loaded drugs time- and pH-dependently as the external pH decreased, while they were stable under physiological conditions at pH 7.4 for over 48 h. The results indicate the micelles should release the loaded drugs in the intracellular acidic regions (pH 5–6) such as endosomes and lysosomes in which the drug-binding hydrazone linkers can be cleaved most effectively. Chemical evidence for absence of free drugs and acid-sensitive cleavage of hydrazone linkers to induce drug release was also presented by RPLC analysis (Figure 2). As described above, ADR is conjugated to amphiphilic block copolymers through pH-sensitive hydrazone linkers. If the drugs were simply entrapped in the micelles by physical interaction instead binding to polymers via chemical linkers, a sharp peak corresponding to the free drug should be separated from drug–polymer conjugates by RPLC and appeared in the physiological condition (pH 7.4) where the acid-labile hydrazone bond remains stable. However, the peak from the free drug was not shown at pH 7.4 but gradually increased in acidic conditions while the broad peak from polymer conjugates decreased. Eventually, almost 100% of the drugs were released at pH 3.0, and on the basis of this, we calculated the drug loading content of polymer conjugate described above. These results demonstrate that acid-sensitive cleavage

Table 1. Growth Inhibitory Effects of the Micelles against Cancer Cells[a]

sample	exposure time (hour)	IC_{50}[b] (μg/mL±SD)	relative index[c]
ADR	3	0.041 ± 0.035	1.05
	10	0.048 ± 0.026	1.23
	24	0.039 ± 0.025	1
micelle	3	1.08 ± 0.12	27.69
	10	0.45 ± 0.061	11.54
	24	0.27 ± 0.038	6.92

[a] Eight independent experiments were carried out using a human small cell lung cancer cell line SBC-3 ($n = 8$). [b] IC_{50} denotes the inhibitory concentration of the drugs required for 50% reduction in cell population. Concentrations of the micelles are calculated with free ADR equivalents. [c] Relative index denotes the ratio between a control and the object for comparison. Here, we evaluated the growth inhibitory effect of the micelles by converting their concentrations with respect to ADR after a 24 h incubation as the control.

of hydrazone linkers between drugs and polymer chains obviously induced drug release.

Regenerated Drugs Were Pharmaceutically Active Inhibiting Cell Growth in Vitro. To verify whether the released drugs are pharmacologically active, an in vitro growth-inhibition test was carried out. The test revealed that the cytotoxic activity of the micelles was as high as 1/7-fold with respect to that of the free drugs after a 24 h exposure time (Table 1). Interestingly, the micelles showed delayed cytotoxicity that was drastically changed depending on the incubation time, which reflects that the drug release from the micelles took place and correlated with the cell metabolism.

The Micelle Infiltrates into the Avascular Tumor Model Multicellular Tumor Spheroids. Recently, it has been reported that the fluorescence quenching effect of the micelles provides a useful tool to observe the intracellular behaviors of the micelles (*22*). The fluorescence intensity of ADR, playing a role not only as an anticancer drug, but also as a fluorescence probe in this study, is quenched due to the locally increased high concentration in the micelle core; however, the fluorescence becomes detectable again as the micelles start to release ADR under acidic conditions. Consequently, the micelles emit intense fluorescence signals with the release of the entrapped ADR; a series of processes such as intracellular trafficking, drug release, and localization were able to be directly monitored in live cells accompanying the structural change. In the meantime, the multicellular tumor spheroid (MCTS) was used as an in vitro tumor model for the experiments because it is the most similar to avascular tumor regions of practical solid tumors in vivo that are characterized by limited accessibility of cell subpopulations (Figure 3). For example, MCTS reproduces adverse microenvironmental conditions of solid tumors in vivo such as hypoxia and nutritional depletion, and the extracellular matrix between tumor cells instead of intratumoral normal cell populations (*27*–*28*).

For these reasons, the intracellular behaviors of the micelles were observed within solid tumors using fluorescence quenching effect and the MCTS. The micelles were coincubated with the MCTS, and the change in the fluorescence intensity was monitored using a confocal laser scanning microscope (CLSM). The three-dimensional CLSM images demonstrated the time-dependent change in the fluorescence intensity of the micelle systems and their distributions throughout the MCTS with a 200 μm diameter depending on the incubation time (Figure 4A). The 200 μm diameter of MCTS was

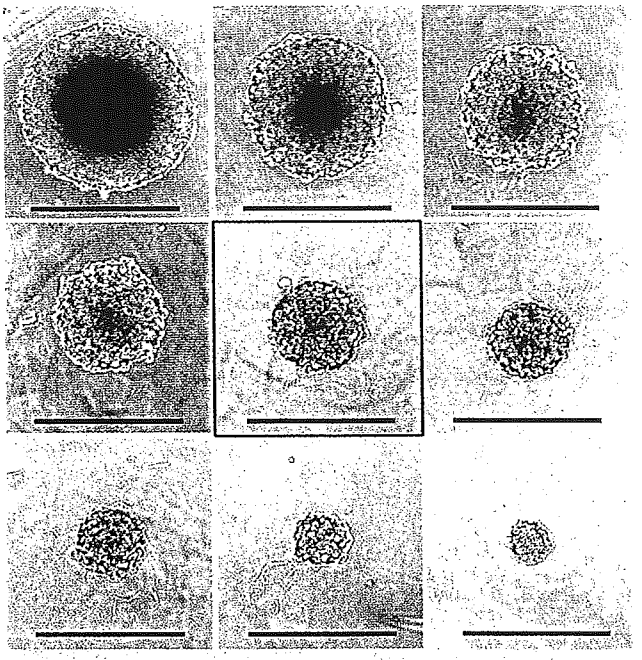

Figure 3. Preparation of multicellular tumor spheroid (MCTS). MCTS with diameter ranging from 100 to 500 μm was prepared from a C26 cell line. Among them, MCTS with a 200 μm diameter (red-edged) was used as an in vitro tumor model because it has the most suitable size for reproducing in vivo avascular tumor regions that are characterized by limited accessibility of cell subpopulations (bar = 500 μm).

determined as the most suitable size for the experiments, considering the fact that the maximum distance between the capillary blood vessels within avascular solid tumor is 200 μm or less (*29*). The fluorescence of the micelle system remained quenched at 1 h after incubation, but it was detected at 3 and 24 h. It is notable that most cell nuclei remained blue at 3 h. The images, therefore, suggest that the micelles began to intracellularly release the drugs but the released drugs were still localized in the cytoplasm. However, the intense fluorescence of ADR was eventually detected in most of the cell nuclei after 24 h. These results reflect that the micelles would access every cell in the avascular region of tumor tissues in vivo to release the drugs.

The Micelles Enter the Cell Interior and Release the Drugs. To get a better understanding of the intracellular distributions of the micelles and their released drugs, further observations of the MCTS coincubated with the micelles under high magnification were carried out using a 63× objective (Figure 4B). These images show clear evidence of the intracellular drug release from the micelles and accumulation of the released drugs in the cell nuclei. The localization of the ADR fluorescence in the cytoplasm after 3 h incubation is supporting our speculation that the micelles internalized the cells releasing the drugs. After additional incubation up to 24 h, the presence of the drugs both in the cytoplasm and cell nuclei was confirmed. When the same experiments were carried out with free ADR, all the cell nuclei in the MCTS became red within 1 h because the ADR with a low molecular weight rapidly penetrated into each cell, and we were not able to observe this unique time-dependent fluorescence change in intensity and its distribution. Therefore, it is obvious that the micelles are precisely functioning in the intracellular regions as we designed, and the possible drug release from the micelles in the extracellular regions is negligible.

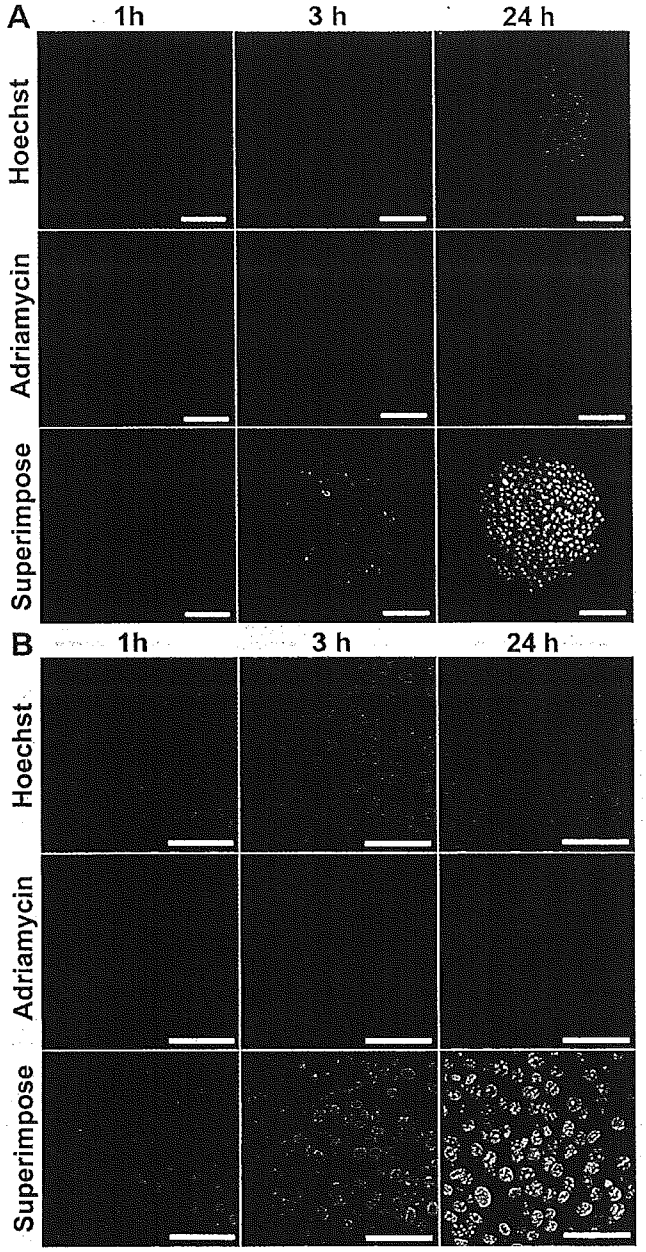

Figure 4. Observation of tumor permeability and intracellular drug release behaviors of the micelles. (A) CLSM observations showed the time-dependent change in the fluorescence intensities of ADR in the micelle system in MCTS. The images showed that the micelles can access the inside of the MCTS and release the loaded drugs (bar = 100 μm). (B) The intracellular drug release and localization of the micelles in each cell of MCTS were observed in detail using a high-magnification 63× objective. The images clearly demonstrated that the micelles internalized into the cells and released drugs, and that the released drugs eventually accumulated in the cell nuclei (bar = 50 μm).

The Micelles Suppress Tumor Growth in Mice with Enhanced Therapeutic Efficacy and Lowered Toxicity. The animal tests revealed that the micelles exerted an effective antitumor activity over a broad range of injection doses to suppress tumor growth in mice, showing some of the clear comparisons with ADR (Figure 5). In the case of ADR, tumor growth was suppressed with a 10 mg/kg dose, but the mice treated with a 15 mg/kg dose were dead due to the drug's toxicity. This corresponds well to the fact that the lethal dose of ADR killing 50% of the test animals within a designated period, called LD_{50}, is generally 12.7−13.2 mg/kg. On the contrary, the micelles were safely injectable up to a 40 mg/kg dose, while three of six mice were completely cured and there was no death among the treated mice. Notably, the body weights of the mice that slightly decreased during the micelle administration recovered, or even increased, on day 30 with respect to the controls (Table 2). Such behavior was not observed in the case of ADR, and the mice were emaciated with a 10 mg/kg dose that was the optimum dose for ADR to suppress tumor growth. Namely, the therapeutic efficacy of the micelles was significantly improved over that of ADR within this animal experiment setting, which distinguishes the micelles from ADR that has a narrow therapeutic window between 10 and 15 mg/kg. In the meantime, the tumor-suppressing antitumor activity of the micelles is shown from a 20 mg/kg dose. The micelles also extended the duration of tumor growth reaching a 5-fold initial tumor volume up to 22 and 28 days for the 20 and 40 mg/kg doses, respectively. These results indicate that the micelles achieved both enhanced therapeutic efficacy and a reduced toxicity of the loaded drugs, which are of great advantage to create effective and safe drug carrier systems.

Table 2. In Vivo Antitumor Activity of the Micelles against C26 Tumor-Bearing Mice

sample	dose (mg/kg)[a]	body weight change on day 30 (%)[b]	toxic death	duration days of tumor growth[c]	complete cure
control	0	−2.18 ± 1.74	0/6	3.7	0/6
ADR	5	−13.35 ± 0.59	0/6	4.2	0/6
	10	−16.84 ± 1.26	0/6	14.6	1/6
	15	–	6/6	–	–
micelle	5	−0.89 ± 1.68	0/6	3.9	0/6
	10	−4.51 ± 1.44	0/6	4.0	0/6
	20	3.13 ± 1.60	0/6	22.1	2/6
	40	−4.07 ± 0.92	0/6	27.9	3/6
	60	–	6/6	–	–

[a] Administrations were carried out three times with a 4-day interval, and doses were determined in free ADR equivalents. [b] Body weights were measured on day 30 after the first injection to compare the long-term toxicity between ADR and the micelles. Values are expressed as mean ± SEM. [c] Duration time to reach 5-fold initial tumor volume.

The Micelles Circulate for a Long Time in the Blood and Selectively Accumulate in Solid Tumors. Effective antitumor activity and low toxicity imply that the micelles are stable in the blood without drug release (or leakage); therefore, their systemic and local distribution may dominate the tumor-suppressing antitumor activity. To demonstrate this, we investigated the in vivo dispositions of the micelles in detail using a biodistribution study. The levels of the micelles in the blood, tumor, and major organs, such as the heart, kidney, liver, and spleen, are expressed as percentage of each dose at specific times after the intravenous injection (Figure 6A). As summarized in Table 3, the micelles circulated in the blood for a prolonged time, and the area under the concentration curve (AUC) of the blood was 15-fold greater than that of ADR. In particular, it is noteworthy that the AUC values of the micelles in the heart and kidney decreased as compared to ADR, indicating that their tumor selectivity (AUC_{tumor}/AUC_{organ}) increased 6- and 5-fold higher with respect to the heart and the kidney, respectively. Such tumor-selective accumulation of the micelles may reduce the side effects of ADR such as cardiotoxicity and nephrotoxicity. In the meantime, the micelles showed a relatively low uptake in the liver and spleen despite the long residence time in the blood in comparison with tumors. These results suggest that the micelles may rapidly evacuate from these reticular

Table 1. Growth Inhibitory Effects of the Micelles against Cancer Cells[a]

sample	exposure time (hour)	IC_{50}[b] (μg/mL±SD)	relative index[c]
ADR	3	0.041 ± 0.035	1.05
	10	0.048 ± 0.026	1.23
	24	0.039 ± 0.025	1
micelle	3	1.08 ± 0.12	27.69
	10	0.45 ± 0.061	11.54
	24	0.27 ± 0.038	6.92

[a] Eight independent experiments were carried out using a human small cell lung cancer cell line SBC-3 ($n = 8$). [b] IC_{50} denotes the inhibitory concentration of the drugs required for 50% reduction in cell population. Concentrations of the micelles are calculated with free ADR equivalents. [c] Relative index denotes the ratio between a control and the object for comparison. Here, we evaluated the growth inhibitory effect of the micelles by converting their concentrations with respect to ADR after a 24 h incubation as the control.

of hydrazone linkers between drugs and polymer chains obviously induced drug release.

Regenerated Drugs Were Pharmaceutically Active Inhibiting Cell Growth in Vitro. To verify whether the released drugs are pharmacologically active, an in vitro growth-inhibition test was carried out. The test revealed that the cytotoxic activity of the micelles was as high as 1/7-fold with respect to that of the free drugs after a 24 h exposure time (Table 1). Interestingly, the micelles showed delayed cytotoxicity that was drastically changed depending on the incubation time, which reflects that the drug release from the micelles took place and correlated with the cell metabolism.

The Micelle Infiltrates into the Avascular Tumor Model Multicellular Tumor Spheroids. Recently, it has been reported that the fluorescence quenching effect of the micelles provides a useful tool to observe the intracellular behaviors of the micelles (*22*). The fluorescence intensity of ADR, playing a role not only as an anticancer drug, but also as a fluorescence probe in this study, is quenched due to the locally increased high concentration in the micelle core; however, the fluorescence becomes detectable again as the micelles start to release ADR under acidic conditions. Consequently, the micelles emit intense fluorescence signals with the release of the entrapped ADR; a series of processes such as intracellular trafficking, drug release, and localization were able to be directly monitored in live cells accompanying the structural change. In the meantime, the multicellular tumor spheroid (MCTS) was used as an in vitro tumor model for the experiments because it is the most similar to avascular tumor regions of practical solid tumors in vivo that are characterized by limited accessibility of cell subpopulations (Figure 3). For example, MCTS reproduces adverse microenvironmental conditions of solid tumors in vivo such as hypoxia and nutritional depletion, and the extracellular matrix between tumor cells instead of intratumoral normal cell populations (*27*–*28*).

For these reasons, the intracellular behaviors of the micelles were observed within solid tumors using fluorescence quenching effect and the MCTS. The micelles were coincubated with the MCTS, and the change in the fluorescence intensity was monitored using a confocal laser scanning microscope (CLSM). The three-dimensional CLSM images demonstrated the time-dependent change in the fluorescence intensity of the micelle systems and their distributions throughout the MCTS with a 200 μm diameter depending on the incubation time (Figure 4A). The 200 μm diameter of MCTS was

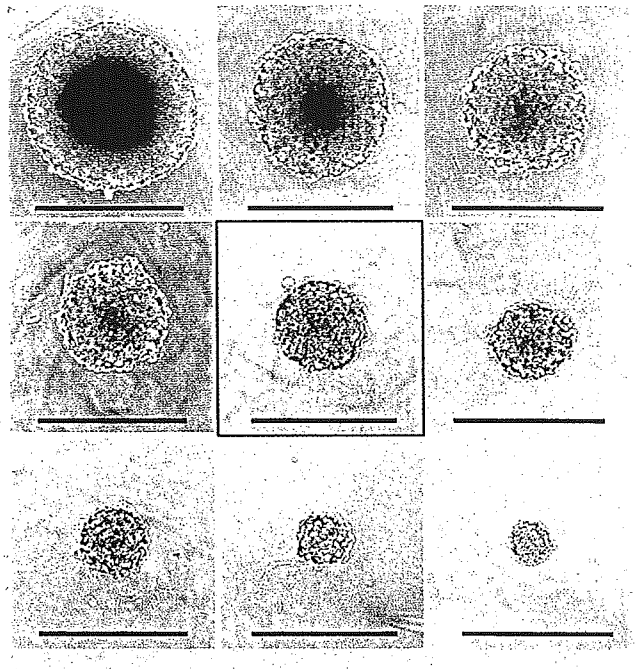

Figure 3. Preparation of multicellular tumor spheroid (MCTS). MCTS with diameter ranging from 100 to 500 μm was prepared from a C26 cell line. Among them, MCTS with a 200 μm diameter (red-edged) was used as an in vitro tumor model because it has the most suitable size for reproducing in vivo avascular tumor regions that are characterized by limited accessibility of cell subpopulations (bar = 500 μm).

determined as the most suitable size for the experiments, considering the fact that the maximum distance between the capillary blood vessels within avascular solid tumor is 200 μm or less (*29*). The fluorescence of the micelle system remained quenched at 1 h after incubation, but it was detected at 3 and 24 h. It is notable that most cell nuclei remained blue at 3 h. The images, therefore, suggest that the micelles began to intracellularly release the drugs but the released drugs were still localized in the cytoplasm. However, the intense fluorescence of ADR was eventually detected in most of the cell nuclei after 24 h. These results reflect that the micelles would access every cell in the avascular region of tumor tissues in vivo to release the drugs.

The Micelles Enter the Cell Interior and Release the Drugs. To get a better understanding of the intracellular distributions of the micelles and their released drugs, further observations of the MCTS coincubated with the micelles under high magnification were carried out using a 63× objective (Figure 4B). These images show clear evidence of the intracellular drug release from the micelles and accumulation of the released drugs in the cell nuclei. The localization of the ADR fluorescence in the cytoplasm after 3 h incubation is supporting our speculation that the micelles internalized the cells releasing the drugs. After additional incubation up to 24 h, the presence of the drugs both in the cytoplasm and cell nuclei was confirmed. When the same experiments were carried out with free ADR, all the cell nuclei in the MCTS became red within 1 h because the ADR with a low molecular weight rapidly penetrated into each cell, and we were not able to observe this unique time-dependent fluorescence change in intensity and its distribution. Therefore, it is obvious that the micelles are precisely functioning in the intracellular regions as we designed, and the possible drug release from the micelles in the extracellular regions is negligible.

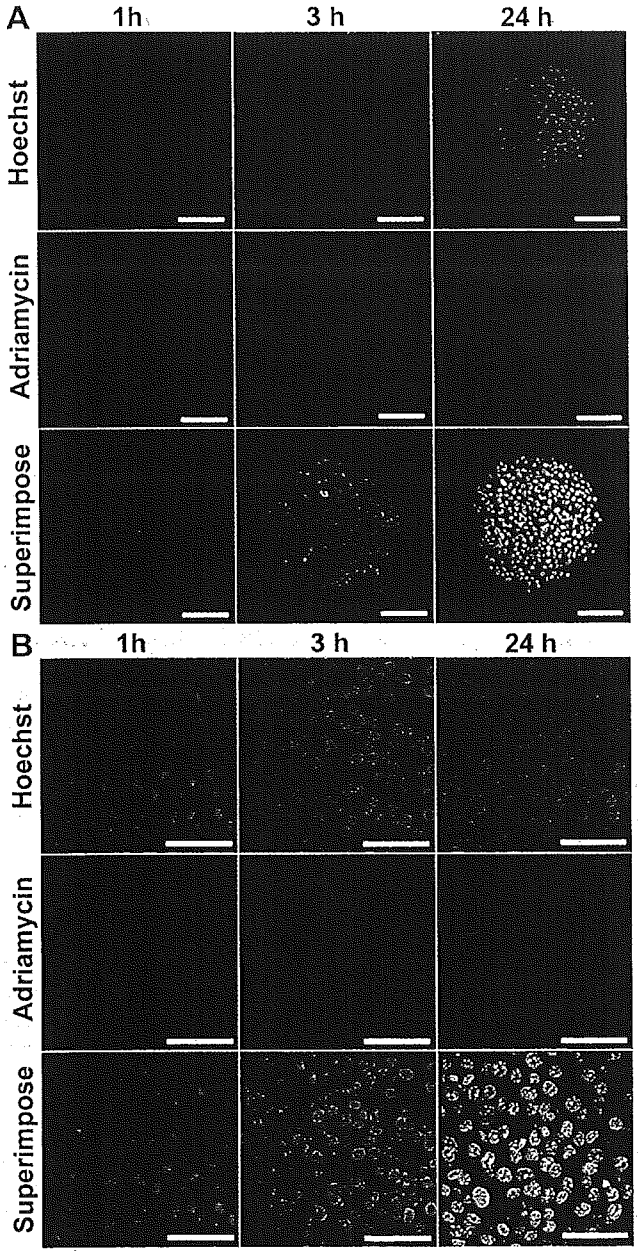

Figure 4. Observation of tumor permeability and intracellular drug release behaviors of the micelles. (A) CLSM observations showed the time-dependent change in the fluorescence intensities of ADR in the micelle system in MCTS. The images showed that the micelles can access the inside of the MCTS and release the loaded drugs (bar = 100 μm). (B) The intracellular drug release and localization of the micelles in each cell of MCTS were observed in detail using a high-magnification 63× objective. The images clearly demonstrated that the micelles internalized into the cells and released drugs, and that the released drugs eventually accumulated in the cell nuclei (bar = 50 μm).

The Micelles Suppress Tumor Growth in Mice with Enhanced Therapeutic Efficacy and Lowered Toxicity. The animal tests revealed that the micelles exerted an effective antitumor activity over a broad range of injection doses to suppress tumor growth in mice, showing some of the clear comparisons with ADR (Figure 5). In the case of ADR, tumor growth was suppressed with a 10 mg/kg dose, but the mice treated with a 15 mg/kg dose were dead due to the drug's toxicity. This corresponds well to the fact that the lethal dose of ADR killing 50% of the test animals within a designated period, called LD_{50}, is generally 12.7−13.2 mg/kg. On the contrary, the micelles were safely injectable up to a 40 mg/kg dose, while three of six mice were completely cured and there was no death among the treated mice. Notably, the body weights of the mice that slightly decreased during the micelle administration recovered, or even increased, on day 30 with respect to the controls (Table 2). Such behavior was not observed in the case of ADR, and the mice were emaciated with a 10 mg/kg dose that was the optimum dose for ADR to suppress tumor growth. Namely, the therapeutic efficacy of the micelles was significantly improved over that of ADR within this animal experiment setting, which distinguishes the micelles from ADR that has a narrow therapeutic window between 10 and 15 mg/kg. In the meantime, the tumor-suppressing antitumor activity of the micelles is shown from a 20 mg/kg dose. The micelles also extended the duration of tumor growth reaching a 5-fold initial tumor volume up to 22 and 28 days for the 20 and 40 mg/kg doses, respectively. These results indicate that the micelles achieved both enhanced therapeutic efficacy and a reduced toxicity of the loaded drugs, which are of great advantage to create effective and safe drug carrier systems.

Table 2. In Vivo Antitumor Activity of the Micelles against C26 Tumor-Bearing Mice

sample	dose (mg/kg)[a]	body weight change on day 30 (%)[b]	toxic death	duration days of tumor growth[c]	complete cure
control	0	−2.18 ± 1.74	0/6	3.7	0/6
ADR	5	−13.35 ± 0.59	0/6	4.2	0/6
	10	−16.84 ± 1.26	0/6	14.6	1/6
	15	–	6/6	–	–
micelle	5	−0.89 ± 1.68	0/6	3.9	0/6
	10	−4.51 ± 1.44	0/6	4.0	0/6
	20	3.13 ± 1.60	0/6	22.1	2/6
	40	−4.07 ± 0.92	0/6	27.9	3/6
	60	–	6/6	–	–

[a] Administrations were carried out three times with a 4-day interval, and doses were determined in free ADR equivalents. [b] Body weights were measured on day 30 after the first injection to compare the long-term toxicity between ADR and the micelles. Values are expressed as mean ± SEM. [c] Duration time to reach 5-fold initial tumor volume.

The Micelles Circulate for a Long Time in the Blood and Selectively Accumulate in Solid Tumors. Effective antitumor activity and low toxicity imply that the micelles are stable in the blood without drug release (or leakage); therefore, their systemic and local distribution may dominate the tumor-suppressing antitumor activity. To demonstrate this, we investigated the in vivo dispositions of the micelles in detail using a biodistribution study. The levels of the micelles in the blood, tumor, and major organs, such as the heart, kidney, liver, and spleen, are expressed as percentage of each dose at specific times after the intravenous injection (Figure 6A). As summarized in Table 3, the micelles circulated in the blood for a prolonged time, and the area under the concentration curve (AUC) of the blood was 15-fold greater than that of ADR. In particular, it is noteworthy that the AUC values of the micelles in the heart and kidney decreased as compared to ADR, indicating that their tumor selectivity (AUC_{tumor}/AUC_{organ}) increased 6- and 5-fold higher with respect to the heart and the kidney, respectively. Such tumor-selective accumulation of the micelles may reduce the side effects of ADR such as cardiotoxicity and nephrotoxicity. In the meantime, the micelles showed a relatively low uptake in the liver and spleen despite the long residence time in the blood in comparison with tumors. These results suggest that the micelles may rapidly evacuate from these reticular

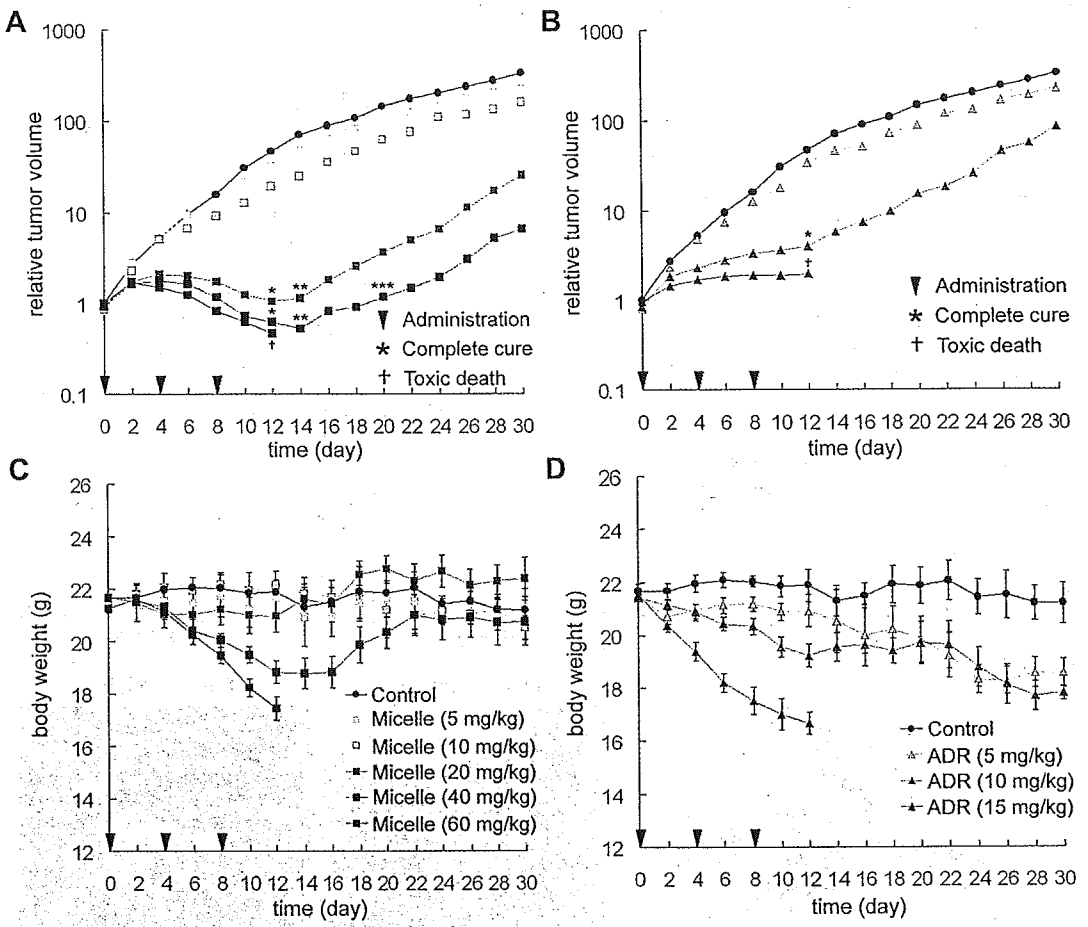

Figure 5. Tumor size and body weight changes of the treated mice. The figures show effective tumor-suppressing activity and low change in body weights over a broad range of injection doses of the micelles (A and C). To the contrary, ADR showed a narrow therapeutic window between 10 and 15 mg/kg does avoiding toxic death (B and D). Administrations were carried out three times with a 4-day interval into tumor bearing CDF1 mice (female, 6-week-old, $n = 6$). The micelle doses are shown as ADR equivalents. Values are expressed as mean and mean ± SEM for the tumor volume and body weight, respectively.

connective tissues without interacting with monocytes and macrophages that are responsible for engulfing and removing cellular debris, old cells, and unwelcome external invaders from the bloodstream. On the contrary, tumor tissues are characterized by a large vascular permeability and high interstitial diffusivity while a lack of lymphatic drainage is observed. This phenomenon is explained by the enhanced permeability and retention (EPR) effect, which significantly affects distributions of the macromolecules facilitating their access and accumulation in tumors (*30, 31*). Consequently, the micelles that accumulated in the solid tumors through the EPR effect can stay for a prolonged time. The biodistribution study, therefore, showed that the cytotoxicity of the micelles seems to depend on their retention time as well as in the accumulated amounts in each organ, which may be crucial in attaining both an effective antitumor activity and reduced toxicity in a single drug carrier system.

In vivo antitumor activity test showed that the micelles effectively suppressed tumor growth in mice over a broad range of injection doses while toxicity remained extremely low. On the other hand, the biodistribution study revealed that the micelles circulated in the blood for a long period of time and accumulated in normal organs as well as the tumors. These results are very interesting because the micelles showed organ-dependent differences in cytotoxicity. To elucidate this, we investigated the localization of the micelles in each organ by calculating the tissue-to-blood concentration ratio K_b (Table 4). The K_b value is defined as [$K_b = C_{tissue}/C_{blood}$] where C_{tissue} and C_{blood} denote the tissue concentration and the blood concentration of the micelles, respectively. Each K_b value indicates distribution of the micelles in vascular space ($K_b < 0.1$), extracellular space ($0.1 < K_b < 0.5$), and intracellular space ($0.5 < K_b$) (*32, 33*). The data revealed that the micelles localized in the cell interior of tumor tissues but mainly distributed in the extracellular space of other organs after accumulation. It is in good accordance with our previous results published elsewhere (*34, 35*). We speculate that such drastic alterations might be due to the pathological differences in vasculatures and lymphatic drainages between organs. Consequently, even though the micelles accumulate in normal organs, they can be excreted from the body before releasing drugs. The organ-dependent cytotoxicity of the micelles, therefore, probably would depend on their retention time as well as the accumulated amounts in each organ.

The Micelles Regulate the Local Drug Distribution within Solid Tumors. In view of their tumor-specific accumulation and intracellular distribution, the micelles should release the drugs in solid tumors along with emitting fluorescence as we observed in the intracellular drug release experiment using MCTS. In contrast, if the micelles released the drugs slowly or not at all, the fluorescence of ADR would remain quenched. On the basis of this hypothesis, we observed the solid tumors and their peripheral blood vessels in mice after intravenous injection of the micelles using a fluorescence microscope (Figure 6B). The observations were carried out at 24 h after injection because the micelles needed to

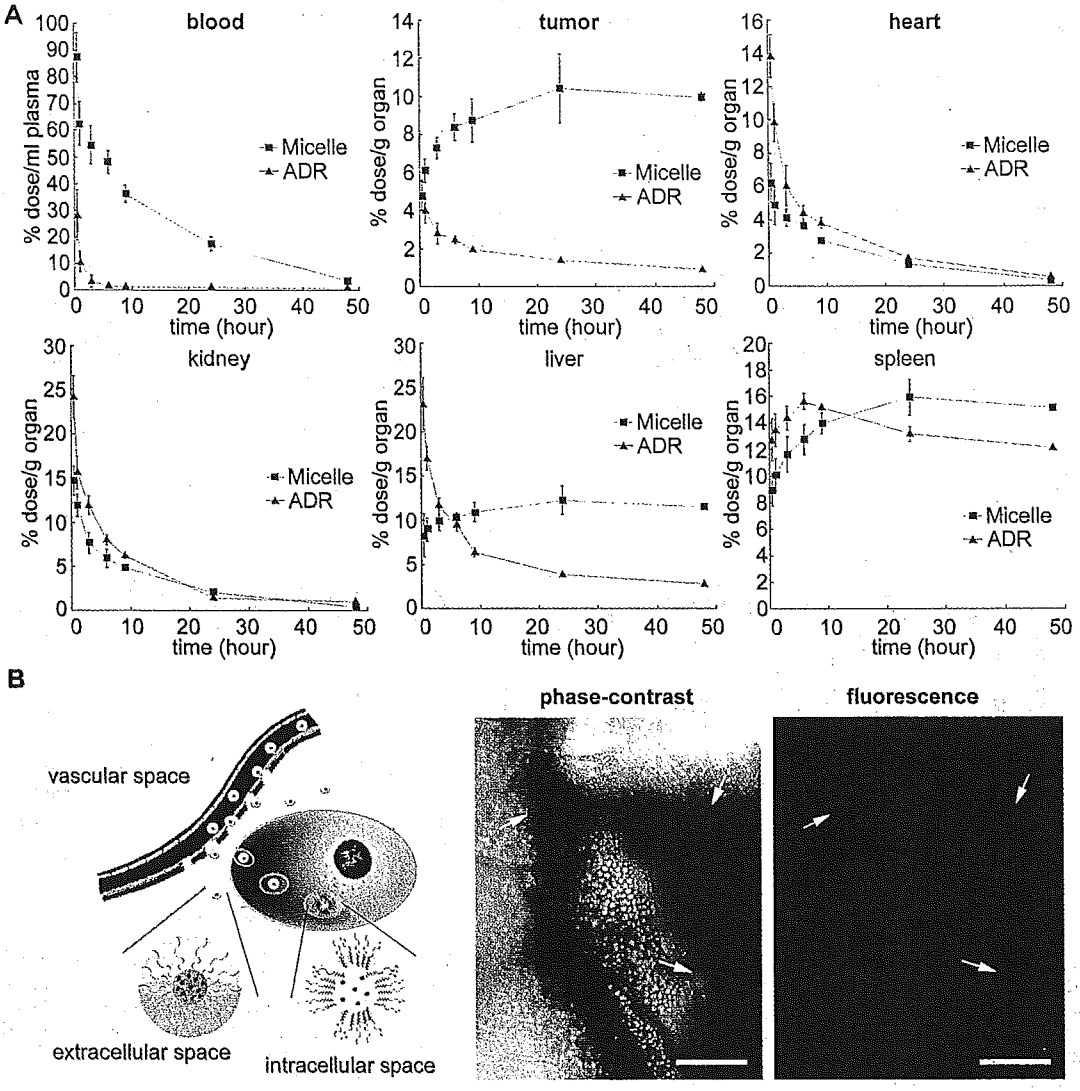

Figure 6. Tumor-specific accumulation of the micelles and locally increased drug concentrations. (A) Biodistribution study revealed the prolonged circulation in the blood and tumor-specific accumulation of the micelles. (B) Fluorescence microscopic observations of the solid tumor and its peripheral regions at 24 h after micelle injection demonstrate that the drug concentrations in the tumor tissues selectively increased due to the tumor-specific accumulation and controlled drug release from the micelles (bar = 500 μm).

Table 3. Tumor-Specific Accumulation of the Micelles

	AUC[a]		AUC ratio	tumor selectivity[b] (AUC_{tumor}/AUC_{organ})		tumor selectivity ratio $[(AUC_{tumor}/AUC_{organ})_{micelle}/(AUC_{tumor}/AUC_{organ})_{ADR}]$
	ADR	micelle	($AUC_{micelle}/AUC_{ADR}$)	ADR	micelle	
blood	58.86	858.54	14.59	–	–	–
tumor	49.59	210.21	4.24	–	–	–
heart	94.70	65.24	0.69	0.52	3.22	6.19
kidney	151.56	117.80	0.78	0.33	1.78	5.39
liver	176.15	261.17	1.48	0.28	0.80	2.86
spleen	341.38	329.66	0.97	0.15	0.64	4.27

[a] AUC denotes the area under a concentration curve that is obtained from the biodistribution study. Values are calculated based on the trapezoidal rule up to 24 h after intravenous injection. [b] Tumor selectivity of ADR and the micelles was determined by calculating the relative accumulated concentrations between the tumor tissues and each organ (AUC_{tumor}/AUC_{organ}). Their ratios indicate the change in the tumor selectivity of the micelles with respect to ADR.

accumulate in the tumor tissues enter the cells and release the drugs intracellularly as long as they were present in the blood. A phase-contrast image showed that the tumor blood vessels containing the micelles begin to leak into the extravascular compartment of the solid tumors (note the red color of the micelles). However, no fluorescence was detected at the corresponding part but in the limited regions of the solid tumor. Therefore, even though colloidal drug carriers are generally considered to localize in the limited peripheral regions of the solid tumors due to poor accessibility, we have confirmed that the micelles can infiltrate into tumor tissues after accumulation, thus increasing the local drug concentration. This conclusion is in good accordance with the results from the permeability testing of the micelles into MCTS.

DISCUSSION

This paper has revealed a new potency of the polymeric micelle drug carrier systems that they can directly deliver drugs to the interior of targeted cells in vivo by infiltrat-

Table 4. Tissue-to-blood Concentration Ratio (K_b) in Each Organ[a]

	organ				
time (h)	tumor	heart	kidney	liver	spleen
0.5	0.0545	0.0714	0.168	0.0946	0.1023
1	0.0976	0.0772	0.1903	0.1429	0.1617
3	0.134	0.0755	0.1402	0.1834	0.2136
6	0.1747	0.0764	0.1226	0.2141	0.2651
9	0.2412	0.0762	0.134	0.3014	0.3859
24	0.5992	0.0761	0.1162	0.7037	0.9158

[a] K_b value is defined as [$K_b = C_{tissue}/C_{blood}$] where C_{tissue} and C_{blood} were the tissue concentration and the blood concentration of the micelles, respectively. Each K_b value indicates the distribution of the drugs in vascular space ($K_b < 0.1$), extracellular space ($0.1 < K_b < 0.5$), and intracellular space ($0.5 < K_b$).

ing into solid tumors. These findings provided a clear answer to the questions whether the nanosized supramolecular drug carriers can access the cells in the avascular region of the solid tumors without structural and functional breakdown, which is also crucial to other intracellular environment-sensitive macromolecular bioconjugates that are injected through the vein for tumor targeting.

For the past several decades, natural and artificial macromolecules have evolved into a very useful class of drug delivery media (*36*–*39*). However, their in vivo applications are not always successful because limited accessibility inside solid tumors causes stagnation of drug carriers at the periphery of the tumor vasculatures, inducing low concentrations of active drugs in the targeted tumor tissues (*40*). Such a poor delivery efficiency of active drugs to the solid tumors is considered a serious problem facing recent cancer therapy using drug carriers. In this regard, we considered that the intrinsic characteristics of drug carriers may play a critical role in determining their in vivo behaviors, such as tumor permeability, drug release property, and antitumor activity. To confirm this, a suitable carrier model is required that controls the release of drugs while its structural features are optimized for a tumor-targeting drug delivery, and we prepared a new type of drug carrier in this study by adding an intracellular pH-triggered drug release property to the polymeric micelle drug carrier system whose chemical and biological properties are clearly identified (*41*).

As shown in the experimental results, the prepared micelle behaves not only as a biocompatible nanosized drug carrier with a high drug-loading content but also as a bioresponsive device with intracellular pH-sensitivity to control the drug release. These characteristic behaviors suggest that the nanosized core–shell structure of the micelles seems important to take the best advantage of the PEG shielding, imparting both stability and fragility into a single carrier system. The micelles safely protect the loaded drugs and functional linkers by providing a nanocompartment in the core that is completely segregated from the external environments; they maintain a high water-solubility with the hydrophilic shell that prevents the adsorption of proteins and the adhesion of cells so as to circumvent the uptake by reticuloendothelial systems during blood circulation (*42*, *43*). In the meantime, intracellular trafficking of the micelles in the solid tumors is evident, which indicates that PEG shielding of the micelle may behave as a kinetic barrier that regulates the condition of the molecular affinity interaction between the micelles and cell membrane according to the exposure or retention time. As explained by the EPR effect, solid tumors feature a large vascular permeability, high interstitial diffusivity, and poor lymphatic drainage; this is a fact that results in tumor-specific retention over a long period of time required for interacting with tumor cells. The retention time in each organ influences the intracellular trafficking of the micelles; thereby, any undesirable cytotoxicity to the normal organs is avoided. Consequently, the intracellular pH-triggered drug release property of the micelles should be the major reason for in vivo antitumor activity with low toxicity.

In conclusion, the intracellular pH-sensitive polymeric micelles exemplify the supramolecular drug carriers that control the systemic, local, and subcellular distribution of the active drugs. They show a higher bioavailability than free drugs, and therefore, the intracellular delivery of drugs would be the most effective and promising formulation for cancer chemotherapy with enhanced therapeutic efficacy and low toxicity. Moreover, the study reveals that the biocompatible structure and environment-sensitive functionality should be considered as a single event in order to realize the carrier systems that are related to these intracellular environments and material transports for the future treatment of cancers with avascular tumor tissue.

ACKNOWLEDGMENT

This research was supported by a Grant-in-Aid for Scientific Research from the Ministry of Education, Culture, Sports, Science and Technology (MEXT), Japan, and by Core Research for Evolutional Science and Technology (CREST), Japan Science and Technology Corporation (JST).

Supporting Information Available: Synthetic scheme for PEG-p(Asp-Hyd-ADR) block copolymer. HPLC analysis protocol for biodistribution. This material is available free of charge via the Internet at http://pubs.acs.org.

LITERATURE CITED

(1) Duncan, R. (2003) The dawning era of polymer therapeutics. *Nat. Rev. Drug Discovery 2*, 347–360.

(2) Maeda, H. (2001) SMANCS and polymer-conjugated macromolecular drugs advantages in cancer chemotherapy. *Adv. Drug Delivery Rev. 46*, 169–185.

(3) Jain, R. K. (2001) Delivery of molecular and cellular medicine to solid tumors. *Adv. Drug Delivery Rev. 46*, 149–168.

(4) Kopecek, J. (2003) Smart and genetically engineered biomaterials and drug delivery systems. *Eur. J. Pharm. Sci. 20*, 1–16.

(5) Nishiyama, N., Okazaki, S., Cabral, H., Miyamoto, M., Kato, Y., Sugiyama, Y., Nishio, K. Matsumura, Y., and Kataoka, K. (2003) Novel cisplatin-incorporated polymeric micelles can eradicate solid tumors in mice. *Cancer Res. 63*, 8977–8983.

(6) Lewanski, C. R. I., and Stewart, S. (1999) PEGylated liposomal adriamycin: a review of current and future applications. *Pharm. Sci. Technol. Today 2*, 473–477.

(7) Jensen, K. D., Nori, A., Tijerina, M., Kopeckova, P., and Kopecek, J. (2003) Cytoplasmic delivery and nuclear targeting of synthetic macromolecules. *J. Controlled Release 87*, 89–105.

(8) Lian, T., and Ho, R. J. Y. (2001) Trends and developments in liposome drug delivery systems. *J. Pharm. Sci. 90*, 667–680.

(9) Kataoka, K., Kwon, G., Yokoyama, M., Okano, T., and Sakurai, Y. (1993) Block-copolymer micelles as vehicles for drug delivery. *J. Controlled Release 24*, 119–132.

(10) Ringsdorf, H. (1975) Structure and properties of pharmacologically active polymers. *J. Polym. Sci. Polym. Symp. 51*, 135–153.

(11) Vasey, P. A., Kaye, S. B., Morrison, R., Twelves, C., Wilson, P., Duncan, R., Thomson, A. H., Murray, L. S., Hilditch, T. E., Murray, T., Burtles, S., Fraier, D., Frigerio, E., and Cassidy, J. (1999) Phase I clinical and pharmacokinetic study of PK1 [N-(2-hydroxypropyl)methacrylamide copolymer doxorubicin]: first member of a new class of chemotherapeutic agents – drug-polymer conjugates. *Clin. Cancer Res. 5*, 83–94.
(12) Gordon, A. N., Fleagle, J. T., Guthrie, D., Parkin, D. E., Gore, M. E., and Lacave, A. J. (2001) Recurrent epithelial ovarian carcinoma: a randomized phase III study of pegylated liposomal doxorubicin versus topotecan. *J. Clin. Oncol. 19*, 3312–3322.
(13) Nakanishi, T., Fukushima, S., Okamoto, K., Suzuki, M., Matsumura, Y., Yokoyama, M., Okano, T., Sakurai, Y., and Kataoka, K. (2001) Development of the polymer micelle carrier system for doxorubicin. *J. Controlled Release 74*, 295–302.
(14) Jain, R. K. (1994) Barriers to drug delivery in solid tumors. *Sci. Am. 271*, 58–65.
(15) Takakura, Y., and Hashida, M. (1996) Macromolecular carrier systems for targeted drug delivery: Pharmacokinetic considerations on biodistribution. *Pharm. Res. 13*, 820–831.
(16) Dvorak, H. F., Nagy, J. A., Dvorak, J. T., and Dvorak, A. M. (1998) Identification and characterization of the blood vessels of solid tumors that are leaky to circulating macromolecules. *Am. J. Pathol. 133*, 95–109.
(17) Ishida, T., Kirchmeier, M. J., Moase, E. H., Zalipsky, S., and Allen, T. M. (2001) Targeted delivery and triggered release of liposomal doxorubicin enhances cytotoxicity against human B lymphoma cells. *Biochim. Biophys. Acta Biomembranes 1515*, 144–158.
(18) Tsukioka, Y., Matsumura, Y., Hamaguchi, T., Koike, H., Moriyasu, F., and Kakizoe, T. (2002) Pharmaceutical and biomedical differences between micellar doxorubicin (NK911) and liposomal doxorubicin (Doxil). *Jpn. J. Cancer Res. 93*, 1145–1153.
(19) Unezaki. S., Maruyama, K., Hosoda, J., Nagae, I., Koyanagi, Y., Nakata, M., Ishida, O., Iwatsuru, M., and Tsuchiya, S. (1996) Direct measurement of the extravasation of poly(ethyleneglycol)-coated liposomes into solid tumor tissue by in vivo fluorescence microscopy. *Int. J. Pharm. 144*, 11–17.
(20) Suzuki, H., Nakai, D., Seita, T., and Sugiyama, Y. (1996) Design of a drug delivery system for targeting based on pharmacokinetic consideration. *Adv. Drug Delivery Rev. 19*, 335–357.
(21) Jones, A. T., Gumbleton, M., and Duncan, R. (2003) Understanding endocytic pathways and intracellular trafficking: a prerequisite for effective design of advanced drug delivery systems. *Adv. Drug Delivery Rev. 55*, 1353–1357.
(22) Bae, Y., Fukushima, S., Harada, A., and Kataoka, K. (2003) Design of environment-sensitive supramolecular assemblies for intracellular drug delivery: polymeric micelles that are responsive to intracellular pH change. *Angew. Chem., Int. Ed. 42*, 4640–4643.
(23) D'souza, A. J. M., and Topp, E. M. (2004) Release from polymeric prodrugs: linkages and their degradation. *J. Pharm. Sci. 93*, 1962–1979.
(24) Ulbrich, K., and Subr, V. (2004) Polymeric anticancer drugs with pH-controlled activation. *Adv. Drug Delivery Rev. 56*, 1023–1050.
(25) Willner, D., Trail, P. A., Hofstead, S. J., King, H. D., Lasch, S. J., Braslawsky, G. R., Greenfield, R. S., Kaneko, T., Firestone, R. A. (1993) (6-Maleimidocaproyl)hydrazone of doxorubicin. A new derivative for the preparation of immunoconjugates of doxorubicin. *Bioconjugate Chem. 4*, 521–527.
(26) Kaneko, T., Willner, D., Monkovic, I., Knipe, J. O., Braslawsky, G. R., Greenfield, R. S., and Vyas D. M. (1991) New hydrazone derivatives of adriamycin and their immunoconjugates – a correlation between acid stability and cytotoxicity. *Bioconjugate Chem. 2*, 133–141.
(27) Hamilton, G. (1998) Multicellular spheroids as an in vitro tumor model. *Cancer Lett. 131*, 29–34.
(28) Sutherland, R. M. (1988) Cell and environment interactions in tumor microregions: the multicell spheroid model. *Science 240*, 177–184.
(29) Konerding, M. A., Fait E., and Gaumann, A. (2001) 3D microvascular architecture of pre-cancerous lesions and invasive carcinomas of the colon. *Br. J. Cancer 84*, 1354–1362.
(30) Maeda, H., Wu, J., Sawa, T., Matsumura, Y., and Hori, K. (2000) Tumor vascular permeability and the EPR effect in macromolecular therapeutics: a review. *J. Controlled Release 65*, 271–284.
(31) Matsumura, Y., and Maeda, H. (1986) A new concept of macromolecular therapeutics in cancer chemotherapy: mechanism of tumoritropic accumulation of proteins and the antitumor agent SMANCS. *Cancer Res. 46*, 6387–6392.
(32) Jain, R. K. (1988) Determinants of tumor blood flow: a review. *Cancer Res. 48*, 2641–2658.
(33) Baxter, L. T., Daniel, H. Z., Mackensen, G., and Jain, R. K. (1994) Physiologically based pharmacokinetic model for specific and nonspecific monoclonal antibodies and fragments in normal tissues and human tumor xenografts in nude mice. *Cancer Res. 54*, 1517–1528.
(34) Yamamoto, Y., Nagasaki, Y., Kato, Y., Sugiyama, Y., and Kataoka, K. (2001) Long-circulating poly(ethylene glycol)-poly(D, L-lactide) block copolymer micelles with modulated surface charge. *J. Control. Release 77*, 27–38.
(35) Nishiyama, N., Kato, Y., Sugiyama, Y., and Kataoka, K. (2001) Cisplatin-loaded polymer–metal complex micelle with time-modulated decaying property as a novel drug delivery system. *Pharmaceut. Res. 18*, 1035–1041.
(36) Torchilin, V. P., Lukyanov, A. N., Gao, Z. G., and Papahadjopoulos-Sternberg, B. (2003) Immunomicelles: Targeted pharmaceutical carriers for poorly soluble drugs. *P. Natl. Acad. Sci. USA. 100*, 6039–6044.
(37) Adams, M. L., Lavasanifar, A., and Kwon, G. (2003) Amphiphilic block copolymers for drug delivery. *J. Pharm. Sci. 92*, 1343–1355.
(38) Shiah, J. G., Dvorak, M., Kopeckova, P., Sun, Y., Peterson, C. M., and Kopecek, J. (2001) Biodistribution and antitumour efficacy of long-circulating N-(2-hydroxypropyl)methacrylamide copolymer-doxorubicin conjugates in nude mice. *Eur. J. Cancer 37*, 131–139.
(39) Kopecek, J., Kopeckova, P., Minko, T., Lu, Z. R., and Peterson, C. M. (2001) Water soluble polymers in tumor targeted delivery. *J. Controlled Release 74*, 147–158.
(40) Emanuel, N., Kedar, E., Bolotin, E. M., Smorodinsky, N. I., and Barenholz, Y. (1996) Targeted delivery of doxorubicin via sterically stabilized immunoliposomes: Pharmacokinetics and biodistribution in tumor-bearing mice. *Pharm. Res. 13*, 861–868.
(41) Kataoka, K., Harada, A., and Nagasaki, Y. (2001) Block copolymer micelles for drug delivery: design, characterization and biological significance. *Adv. Drug. Delivery Rev. 47*, 113–131.
(42) Yokoyama, M., Okano, T., Sakurai, Y., Fukushima, S., Okamoto, K., and Kataoka, K. (1999) Selective delivery of adriamycin to a solid tumor using a polymeric micelle carrier system. *J. Drug Target. 7*, 171–186.
(43) Kwon, G., Suwa, S., Yokoyama, M., Okano, T., Sakurai, Y., and Kataoka, K. (1994) Enhanced tumor accumulation and prolonged circulation times of micelle-forming poly(ethylene oxide-aspartate) block copolymer-adriamycin conjugates. *J. Controlled Release 29*, 17–23.

BC0498166

British Journal of Cancer (2005) 92, 1240–1246

www.bjcancer.com

NK105, a paclitaxel-incorporating micellar nanoparticle formulation, can extend *in vivo* antitumour activity and reduce the neurotoxicity of paclitaxel

T Hamaguchi[1], Y Matsumura[*,1,2], M Suzuki[3], K Shimizu[3], R Goda[3], I Nakamura[3], I Nakatomi[4], M Yokoyama[5], K Kataoka[6] and T Kakizoe[7]

[1]Department of Medicine, President of National Cancer Center, 5-1-1 Tsukiji, Chuo-ku, Tokyo 104-0045, Japan; [2]Investigative Treatment Division, National Cancer Center Research Institute East, 6-5-1 Kashiwanoha, Kashiwa, Chiba 277-8577, Japan; [3]Pharmaceuticals Group, Research & Development Division, Nippon Kayaku Co., Ltd, 3-31-12 Shimo, Kita-ku, Tokyo 115-8588, Japan; [4]NanoCarrier Co., Ltd, Tokatsu Techno Plaza, 5-4-6 Kashiwanoha, Kashiwa, Chiba 277-0882, Japan; [5]Kanagawa Academy of Science and Technology, KSP Bldg., East 404, 3-2-1 Sakado, Takatsu-ku, Kawasaki, Kanagawa 213-0012, Japan; [6]Department of Materials Engineering, Graduate School of Engineering, The University of Tokyo, 7-3-1 Hongo, Bunkyo-ku, Tokyo 113-8656, Japan; [7]President of National Cancer Center, 5-1-1 Tsukiji, Chuo-ku, Tokyo 104-0045, Japan

Paclitaxel (PTX) is one of the most effective anticancer agents. In clinical practice, however, high incidences of adverse reactions of the drug, for example, neurotoxicity, myelosuppression, and allergic reactions, have been reported. NK105, a micellar nanoparticle formulation, was developed to overcome these problems and to enhance the antitumour activity of PTX. Via the self-association process, PTX was incorporated into the inner core of the micelle system by physical entrapment through hydrophobic interactions between the drug and the well-designed block copolymers for PTX. NK105 was compared with free PTX with respect to their *in vitro* cytotoxicity, *in vivo* antitumour activity, pharmacokinetics, pharmacodynamics, and neurotoxicity. Consequently, the plasma area under the curve (AUC) values were approximately 90-fold higher for NK105 than for free PTX because the leakage of PTX from normal blood vessels was minimal and its capture by the reticuloendothelial system minimised. Thus, the tumour AUC value was 25-fold higher for NK105 than for free PTX. NK105 showed significantly potent antitumour activity on a human colorectal cancer cell line HT-29 xenograft as compared with PTX ($P<0.001$) because the enhanced accumulation of the drug in the tumour has occurred, probably followed by its effective and sustained release from micellar nanoparticles. Neurotoxicity was significantly weaker with NK105 than with free PTX. The neurotoxicity of PTX was attenuated by NK105, which was demonstrated by both histopathological ($P<0.001$) and physiological ($P<0.05$) methods for the first time. The present study suggests that NK105 warrants a clinical trial for patients with metastatic solid tumours.
British Journal of Cancer (2005) **92,** 1240–1246. doi:10.1038/sj.bjc.6602479 www.bjcancer.com
Published online 22 March 2005

Keywords: NK105; paclitaxel; polymer micelles; DDS; EPR effect

Paclitaxel (PTX) is one of the most useful anticancer agents known for various cancers including ovarian, breast, and lung cancers (Carney, 1996; Khayat *et al*, 2000). However, PTX has serious adverse effects, for example, neutropenia and peripheral sensory neuropathy. In addition, anaphylaxis and other severe hypersensitive reactions have been reported to develop in 2–4% of patients receiving the drug even after premedication with antiallergic agents; these adverse reactions have been attributed to the mixture of Cremophor EL and ethanol, which was used to solubilise PTX (Weiss *et al*, 1990; Rowinsky and Donehower, 1995). Of the adverse reactions, neutropenia can be prevented or managed effectively by administering a granulocyte colony-stimulating factor. On the other hand, there are no effective therapies to prevent or reduce nerve damage, which is associated with peripheral neuropathy caused by PTX; therefore, neurotoxicity constitutes a significant dose-limiting toxicity of the drug (Rowinsky *et al*, 1993; Wasserheit *et al*, 1996).

The above problems of PTX have been attributed to its low therapeutic indices and limited efficacy due to the nonselective nature of its therapeutic targets and its inability to accumulate selectively in cancer tissue. Therefore, there is an urgent need to develop modalities by which cytotoxic drugs can selectively target tumour tissue and effectively act on cancer cells in the scene. The roles of drug delivery systems (DDSs) have drawn attention in this context. Drug delivery systems are based on two main principles: active and passive targetings. The former refers to the development of monoclonal antibodies directed against tumour-related molecules that allow targeting of the tumour because of specific binding between the antibody and its antigen. However, the application of

*Correspondence: Dr Y Matsumura, Investigative Treatment Division, National Cancer Center Research Institute East, 6-5-1 Kashiwanoha, Kashiwa, Chiba 277-8577, Japan; E-mail: yhmatsum@east.ncc.go.jp
Received 27 October 2004; revised 26 January 2005; accepted 31 January 2005; published online 22 March 2005

DDSs using monoclonal antibodies is restricted to tumours expressing high levels of related antigens.

Passive targeting is based on the so-called enhanced permeability and retention (EPR) effect (Matsumura and Maeda, 1986; Maeda *et al*, 2000). The EPR effect consists in the pathophysiological characteristics of solid tumour tissue: hypervascularity, incomplete vascular architecture, secretion of vascular permeability factors stimulating extravasation within cancer tissue, and absence of effective lymphatic drainage from tumours that impedes the efficient clearance of macromolecules accumulated in solid tumour tissues.

Several techniques to maximally use the EPR effect have been developed, that is, modification of drug structures and development of drug carriers. The first micelle-forming polymeric drug developed was polyethylene glycol (PEG)-polyaspartate block copolymer conjugated with doxorubicin (DXR) (Yokoyama *et al*, 1990; Yokoyama *et al*, 1991; Kataoka *et al*, 1993). PEG constituted the outer shell of the micelle, which conferred a stealth property on the drug that allowed the micellar drug preparations to be less avidly taken up by the reticuloendothelial system (RES) and to be retained in the circulation for a longer time. Prolonged circulation time and the ability of polymeric micelles to extravasate through the leaky tumour vasculature were expected to result in the accumulation of DXR in tumour tissue due to the EPR effect (Kwon *et al*, 1994; Yokoyama *et al*, 1999). A clinical trail of micellar DXR, NK911, is now underway (Nakanishi *et al*, 2001; Hamaguchi *et al*, 2003). Recently, we succeeded in constructing NK105, a polymeric micelle carrier system for PTX, which conferred on PTX a passive targeting ability based on the EPR effect. In the present paper, we describe the details and characteristics of NK105. We also discuss differences between NK105 and other DDS formulations containing PTX.

MATERIALS AND METHODS

Materials

PTX was purchased from Mercian Corp. (Tokyo, Japan). All other chemicals were of reagent grade. Following cell lines, MKN-45, MKN-28, HT-29, DLD-1, HCT116, TE-1, TE-8, PC-14, PC-14/TXT, H460, MCAS, OVCAR-3, AsPC-1, PAN-9, PAN-3, and MCF-7 cells were purchased from American Type Culture Collection. Colon 26 cells were dispensed from the Japan Foundation for Cancer Research (Tokyo, Japan). Female BALB/c *nu/nu* mice were purchased from SLC (Shizuoka, Japan). Female CDF1 mice and IGS rats were purchased from Charles River Japan Inc. (Kanagawa, Japan).

All animal procedures were performed in compliance with the guidelines for the care and use of experimental animals, which had been drawn up by the Committee for Animal Experimentation of the National Cancer Center; these guidelines meet the ethical standards required by law and also comply with the guidelines for the use of experimental animals in Japan.

NK105, a PTX-incorporating micellar nanoparticle formulation

NK105 is a PTX-incorporating 'core-shell-type' polymeric micellar nanoparticle formulation. Polymeric micellar particles were formed by facilitating the self-association of amphiphilic block copolymers in an aqueous medium. Novel amphiphilic block copolymers, namely NK105 polymers, were designed for PTX entrapment. NK105 polymers were constructed using PEG as the hydrophilic segment and modified polyaspartate as the hydrophobic segment. Carboxylic groups of polyaspartate block were modified with 4-phenyl-1-butanol by esterification reaction, consequently the half of the groups were converted to 4-phenyl-1-butanolate. Via the self-association process, PTX was incorporated into the inner core of the micelle system by physical entrapment through hydrophobic interactions between the drug and specifically well-designed block copolymers for PTX.

Pharmacokinetics and pharmacodynamics of PTX and NK105

Colon 26 tumour-bearing CDF1 mice aged 8 weeks were given intravenously (i.v.) via the tail vein PTX 50 and 100 mg kg^{-1} or NK105 at corresponding PTX-equivalent doses. Mice were killed at 5 and 30 min, as well as 2, 6, 24, and 72 h after injection. Blood was collected, and tumours were removed; plasma and tumours obtained were then stored at −20°C until the analysis. Each time point for collection represented three samples from three different mice. PTX was extracted from plasma obtained by deproteinisation using acetonitrile, followed by liquid–liquid extraction with *t*-butylmethylether. Tumours obtained were homogenised in 0.5% acetic acid, and the resultant homogenate was deproteinised and extracted according to the same method as that used for plasma. The blood and tumour extracts were analysed for PTX by liquid chromatography/tandem mass spectrometry. Reversed-phase column-switching chromatography was conducted using an ODS column and detection was enabled by electrospray ionisation of positive mode. The mean plasma and tumour concentrations of PTX at each sampling point were calculated for both PTX and NK105. Pharmacokinetic modelling was completed using a WinNonlin Standard software version 3.1 (Pharsight Corp., California, USA).

In vitro cytotoxicity

Various human cancer cell lines were evaluated in the present study. The cell lines were maintained in monolayer cultures in Dulbecco's modified Eagle's medium containing 10% (v v^{-1}) foetal calf serum and 600 mg l^{-1} glutamine. WST-8 Cell Counting Kit-8 (Dojindo, Kumamoto, Japan) was used for the cell proliferation assay. In all, 2000 cells of each cell line in 90 μl of culture medium were plated in 96-well plates and were then incubated for 24 h at 37°C. Serial dilutions of PTX or NK105 in a volume of 10 μl were added, and the cells were incubated for 48 or 72 h. All data were expressed as mean ± s.e. of triplicate cultures. The data were then plotted as a percentage of the data from the control cultures, which were treated identically to the experimental cultures, except that no drug was added.

Evaluation of the antitumour activity of PTX and NK105

The antitumour activity of PTX and NK105 was evaluated using nude mice implanted with a human colonic cancer cell line, HT-29. One million tumour cells of HT-29 were inoculated at a subcutaneous (s.c.) site on the back skin of BALB/c female nude mice aged 6 weeks. When tumour size reached approximately 5–8 mm in diameter, mice were randomly allocated to the PTX administration group, NK105 administration group, and control administration group, each of which was made up of five animals. Each treatment was carried out as follows: free PTX group was administered at a dose of 25, 50, or 100 mg kg^{-1}; NK105 group was with same PTX-equivalent doses; and in control group, animals were given saline. Mice were administered a single i.v. injection of PTX or NK105 weekly for 3 weeks. The antitumour activity of PTX and NK105 was evaluated by measuring tumour size ($a \times b$, where a is the major diameter and b is the minor diameter) at various time points after injection. Changes in body weight were also monitored for mice, which were used in the present study.

Evaluation of neurotoxicity

The severity of neurotoxicity was assessed both electrophysiologically and histologically. Under intraperitoneal ketamine anaesthesia (40 mg kg^{-1}), rats were given a single i.v. injection of PTX (7.5 mg kg^{-1}), NK105 (a PTX-equivalent dose of 7.5 mg kg^{-1}), or 5% glucose weekly for 6 weeks. All the solutions were administered through the jugular vein exposed via a small incision in the neck. Electrophysiological measurements were conducted 1 day before the first dosing and on day 6 after the final dosing. For electrophysiological recording, rats were anaesthetised by the intraperitoneal injection of pentobarbital 40 mg kg^{-1}. Electrical stimuli were given peripherally, and caudal sensory nerve action potentials (caudal SNAPs) were recorded centrally from the tail. The amplitude of each waveform was calculated by measuring the caudal SNAP from the top peak to the bottom peak. Variations in the amplitude after the 6th weekly administration of the solutions were determined.

For light microscopy, rats were killed after electrophysiological recordings. Subsequently, a segment of the sciatic nerve was carefully removed, and embedded in paraffin. Sections (2 μm thick) were stained with haematoxylin and eosin (H & E) before examination under light microscopy to evaluate the degenerative changes of myelinated nerve fibres.

Statistical analysis

The data of therapeutic efficacy was expressed as mean$\pm$s.e.m. The statistical significance of differences in therapeutic efficacy between two administration groups was calculated by means of repeated measures (analysis of variance). The statistical significance of the differences in neurotoxic activity between two administration groups was calculated using the Student's t-test on the closed testing procedure. The histopathological impairment was scored in five grades. The statistical significance of the differences in histopathological impairment between two administration groups was calculated using the Wilcoxon's rank-sum test on the closed testing procedure. All data were calculated with software StatView, version 5 (ABACUS Concepts, Berkeley, CA, USA). A value of $P<0.05$ was considered statistically significant.

RESULTS

Preparation and characterisation of NK105

To construct NK105 micellar nanoparticles (Figure 1A), block copolymers consisting of PEG and polyaspartate, the so-called PEG polyaspartate described previously (9, 11, 13, 14), were used. PTX was incorporated into polymeric micelles formed by physical entrapment utilising hydrophobic interactions between PTX and the block copolymer polyaspartate chain. After screening of many candidate substances, 4-phenyl-1-butanol was employed for the chemical modification of the polyaspartate block to increase its hydrophobicity. Treating with a condensing agent, 1,3-diisopropylcarbodiimide, the half of carboxyl groups on the polyaspartate, was esterified with 4-phenyl-1-butanol. Molecular weight of the polymers was determined to be approximately 20 000 (PEG block: 12 000; modified polyaspartate block: 8000). NK105 was prepared by facilitating the self-association of NK105 polymers and PTX. NK105 was obtained as a freeze-dried formulation and contained ca. 23% (w w^{-1}) of PTX, as determined by reversed-phase liquid chromatography using an ODS column with mobile phase consisting of acetonitrile and water (9 : 11, v v^{-1}) and detection of ultraviolet absorbance at 227 nm. Finally, NK105, a PTX-incorporating polymeric micellar nanoparticle formulation with a single and narrow size distribution, was obtained. The weight-average diameter of the nanoparticles was approximately 85 nm ranging from 20 to 430 nm (Figure 1B).

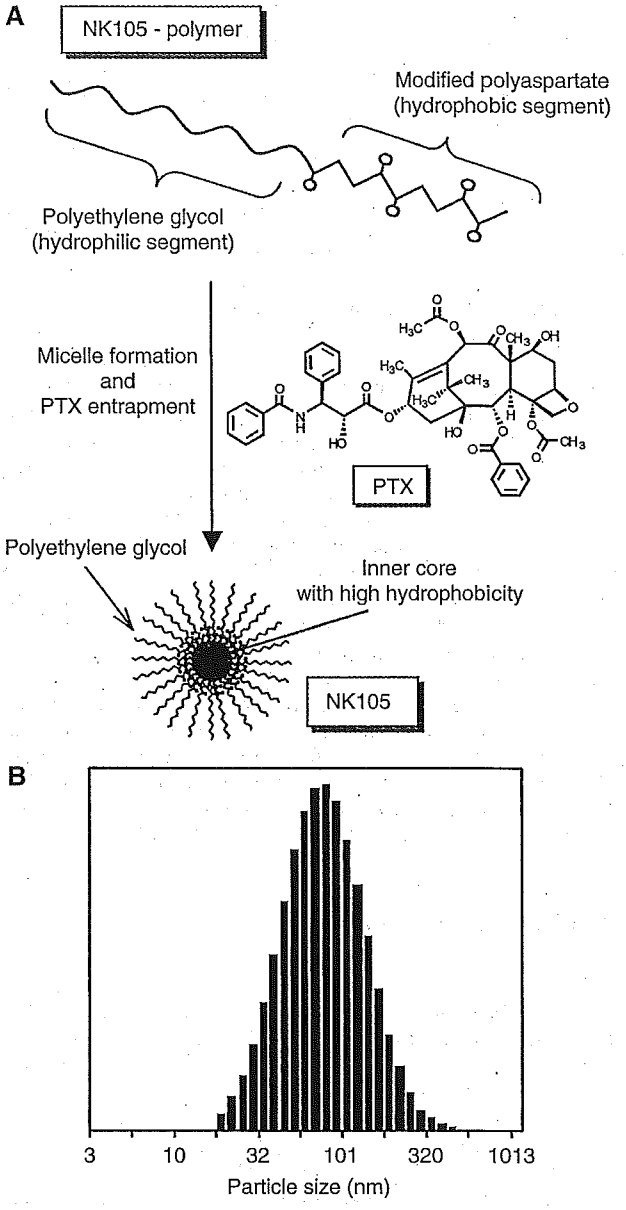

Figure 1 Preparation and characterisation of NK105. (**A**) The micellar structure of NK105 PTX was incorporated into the inner core of the micelle. (**B**) The size distribution of NK105 measured by the dynamic light scattering method. The mean diameter of an NK105 micelle was 85 nm.

Pharmacokinetics and pharmacodynamics of NK105

Colon 26-bearing CDF1 mice were given a single i.v. injection of PTX 50 or 100 mg kg^{-1}, or of NK105 at an equivalent dose of PTX. Subsequently, the time-course changes in the plasma and tumour levels of PTX were determined in the PTX and NK105 administration groups (Figure 2); furthermore, the pharmacokinetic parameters of each group were also determined (Table 1). NK105 exhibited slower clearance from the plasma than PTX, while NK105 was present in the plasma for up to 72 h after injection; PTX was not detected after 24 h or later of injection. The plasma concentration at 5 min ($C_{5\,min}$) and the area under the curve (AUC) of NK105 were 11–20-fold and 50–86-fold higher for NK105 than for PTX, respectively. Furthermore, the half-life at the terminal phase ($t_{1/2}z$) was 4–6 times longer for NK105 than for